Cubic inclusions in hexagonal AlN, GaN, and InN: Electronic states

A. Belabbes,[*] L. C. de Carvalho, A. Schleife, and F. Bechstedt[†]

Institut für Festkörpertheorie und -optik, Friedrich-Schiller-Universität and European Theoretical Spectroscopy Facility (ETSF), Max-Wien-Platz 1, DE-07743 Jena, Germany

(Received 18 February 2011; revised manuscript received 23 May 2011; published 7 September 2011)

Modern quasiparticle calculations based on hybrid functionals and the GW approximation or a transition-state approach are used to predict natural band discontinuities between wurtzite and zinc-blende polytypes of AlN, GaN, and InN by two alignment methods, a modified Tersoff method for the branch-point energy and the Shockley-Anderson model aligning electrostatic potentials. We find a type-I heterostructure behavior for cubic layers embedded in wurtzite for GaN and InN, while AlN tends to a type-II heterostructure behavior. In addition, the electronic states of wurtzite-zinc-blende superlattices are studied in detail with respect to their energy position and wave-function localization. While the lowest electron states are localized in the cubic inclusion for all nitrides, the localization of the uppermost hole states is less clear but tends to be in the hexagonal matrix. The influence of the built-in internal electric fields is discussed.

DOI: 10.1103/PhysRevB.84.125108 PACS number(s): 71.15.Qe, 71.20.Nr, 73.21.Cd

I. INTRODUCTION

The group-III nitrides AlN, GaN, and InN have acquired technological importance for light-emitting and laser-diode as well as electronic-device applications. The three nitrides crystallize in wurtzite (wz) structure under ambient conditions.[1] Strain-free wz crystals belong to the $P6_3mc$ (C_{6v}^4) space group. Therefore, a key property of wz nitrides is their large spontaneous polarization field,[2,3] which allows an additional tailoring of electronic properties. However, the group-III nitrides can also be grown in zinc-blende (zb) structure by means of different epitaxy techniques such as molecular beam epitaxy (MBE).[4] The corresponding space group is $F\bar{4}3m$ (T_d^2). Figure 1 depicts possible unit cells of wz and zb structures. In [0001] direction, wz is characterized by the stacking sequence ABABAB... with each repeated period perpendicular to the basal plane, whereas zb has the sequence ABCABC... in [111] direction. Each letter stands for a bilayer, an ordered pair of cation and anion layers. The letters A, B, and C indicate different hexagonal points, i.e., lateral positions of the bilayers as shown in Fig. 1. Taking the crystal system, hexagonal (H) or cubic (C) and the translational symmetry in stacking direction into account, one also speaks about $2H$ (wz) and $3C$ (zb) polytypes. A consequence of the polytypism can be stacking faults or cubic inclusions in the hexagonal matrix of AlN, GaN, and InN.[5,6] Such extended defects have also been studied theoretically, e.g. by first-principles calculations of stacking-fault formation energies[7] or the consequences for the electronic states.[8]

In the search of new concepts for the reduction of power consumption in large-scale integrated circuits, nanowires (NWs) in which the device size is even further reduced are intensively studied. Moreover, semiconductor NWs are emerging as versatile building blocks for photonic devices. Such nanorods have also been successfully made of nominally wz nitrides.[9–11] Theoretical studies using empirical methods[12] suggest the existence of critical NW diameters, where the NW stackings turn out to be bistable forming both wz and zb structures if zb is energetically more stable than wz in bulk. This bistability has been studied for several common III-V compounds (see e.g. Ref. 13). Recently, it has been demonstrated experimentally that nitride NWs (e.g. made by GaN) can be grown as cubic polytype by plasma-assisted MBE despite that the wz is favored in bulk.[14] The corresponding luminescence lines in zb GaN are shifted toward lower energies by 0.2 eV with respect to wz GaN. However, there is also an intense luminescence peak in between, which is attributed to excitons bound to stacking faults that form at the cubic-hexagonal interface. Stacking changes have been also observed by other groups.[15]

The observation of a stacking variation in [0001]/[111] direction suggests the possibility of polytypic superlattices or, in general, heterocrystalline structures[16] also for the group-III nitrides. Their properties are determined by the electronic states in the entire system and the line-up of the allowed empty or occupied bands at the interface between the wz and zb polytypes depicted in Fig. 1. The key questions concern the magnitude and sign of the band discontinuities between wz matrix and cubic inclusion, especially the localization of the highest occupied or lowest empty electronic states in a heterocrystalline but homomaterial system. In the present paper, these questions are answered using the most modern electronic-structure theory.

II. COMPUTATIONAL METHODS

A. Atomic structures

The atomic geometries of the underlying zb and wz polytypes as well as the superlattices that model the heterocrystalline structures are derived from total-energy minimizations within the *ab initio* density-functional theory (DFT). The exchange-correlation (XC) functional is described within a semilocal approximation, more precisely the generalized-gradient approximation (GGA). We use the novel AM05 functional,[17] which gives excellent results for the structural and elastic properties of group-III nitrides.[18] All DFT calculations are performed within the implementation in the Vienna *ab initio* simulation package (VASP).[19] The pseudopotentials are generated by means of the projector-augmented-wave (PAW) method[20] that allows for the accurate treatment of the valence s and p electrons as well as the semicore Ga $3d$ and In $4d$ states. In the regions between the cores, the wave functions are expanded in plane waves up to a kinetic-energy cutoff

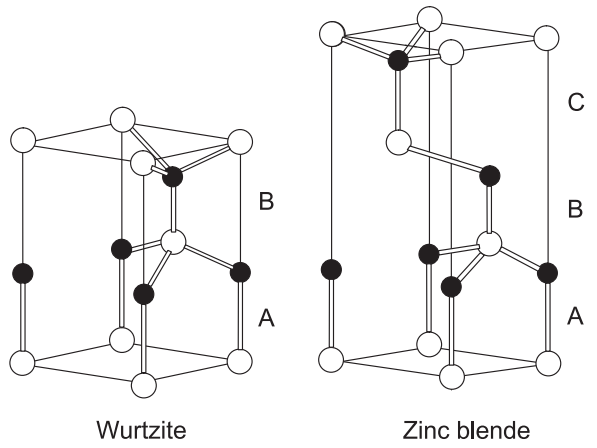

FIG. 1. Wurtzite (a) and zinc-blende (b) structures. Primitive (wz) and nonprimitive (zb) hexagonal unit cells are shown. Open circles and black dots denote cations and anions, respectively.

of 500 eV. The Brillouin zone (BZ) is sampled with a mesh of $8 \times 8 \times 8$ or $8 \times 8 \times 6$ (AlN) and $16 \times 16 \times 16$ or $16 \times 16 \times 12$ (GaN and InN) Monkhorst-Pack (MP) $\mathbf{k}$ points[21] in the zb or wz case. The resulting cubic lattice constants are $a_0 = 4.37$, 4.50, and 5.01 Å for AlN, GaN, and InN, while the hexagonal lattice constants amount to $a = 3.11$, 3.18, and 3.55 Å as well as $c = 4.98$, 5.18, and 5.74 Å. The internal-cell parameters are $u = 0.380$, 0.376, and 0.377. The stabilization energies, i.e., the total-energy differences ΔE_{zb-wz} per cation-anion pair, $\Delta E_{zb-wz} = 47$, 15, and 24 meV do not show a clear chemical trend.

For the superlattices the number of MP mesh points in the BZ is reduced to $16 \times 16 \times 1$. The superlattices used are illustrated in Fig. 2. We study superlattices with 18 cation-anion bilayers, $(2H)_6(3C)_2$ with cubic inclusions of thickness $D \approx 2\sqrt{3}a_0 \approx 3c$ and a total superlattice period of $d \approx 9c$. The lattice constants of the two polytypes differ in the plane perpendicular to the c axis. Since the vertical extent of the cubic inclusions is much smaller than that of the matrix, we allow a small biaxial strain in the cubic layers by fixing the a lattice constant to the $2H$ value. More precisely, a small biaxial strain due to the lateral lattice misfit of a (wz) and $a_0/\sqrt{2}$ (zb) of about 0.6, 0.1, and 0.3% for AlN, GaN, and InN is taken into account. The bilayer thickness of the cubic inclusions is then set to $\sqrt{\frac{2}{3}}a$ (assuming an almost ideal c/a ratio), which leads to a lattice constant of $d = 6(c + \sqrt{\frac{2}{3}}a)$ of the superlattices. We study cubic inclusions $(3C)_2$ with 6 bilayers embedded in $(2H)_6$ in order to directly compare to $(2H)_9$ superlattices of pure wurtzite. Such a comparison may indicate the energetic position of electronic states of the cubic inclusions $(3C)_2$ instead of $(2H)_3$ near the band edges around the fundamental gap of $2H$ after an appropriate energy alignment by means of the electrostatic potentials.

B. Quasiparticle electronic structure

The Kohn-Sham eigenvalues of the DFT[19,20] cannot be identified with the energies of single electronic excitations. Instead, the quasiparticle (QP) equation with a spatially non-local, non-Hermitian, and energy-dependent XC self-energy operator has to be solved.[22,23] In the last years, an

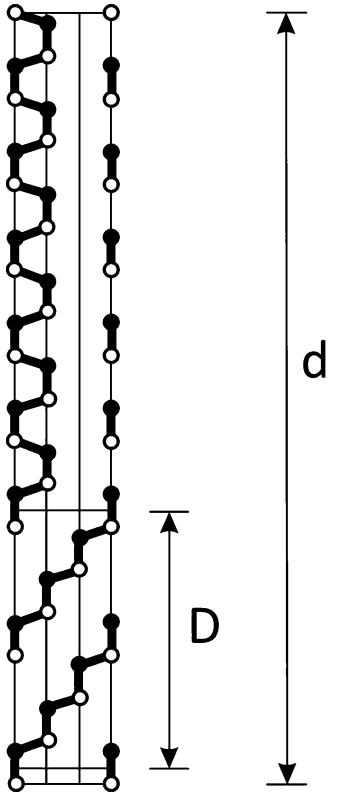

FIG. 2. Structure of the unit cell of a $(2H)_6(3C)_2$ superlattice that model the cubic inclusion in the hexagonal matrix. The bond stacking is shown in the $(11\bar{2}0)$ plane. The nominal interfaces are indicated by horizontal lines.

efficient method based on Hedin's GW approximation[22,23] has been developed[24] to achieve an iterative solution of the QP equation. Replacing the XC self-energy by the functional derivative of the non-local HSE06 hybrid functional[25–27] (using a parameter of $\omega = 0.15$ a.u.$^{-1}$ instead of $\omega = 0.11$ a.u.$^{-1}$, see disambiguation in Ref. 28) provides a zeroth approximation that gives eigenvalues and eigenfunctions close to the final QP quantities.[29] Thereby, we are using the PBE pseudopotentials[30] generated for the GGA XC functional. After the first iteration of the QP equation. eigenvalues are obtained (cf. Table I) that give energy gaps that are, e.g. for nitrides, close to the experimental values.[18,31]

For wz-zb superlattices with about 36 atoms in the unit cell, the above-described method is too expensive, especially because of the spatially non-local starting point and the convergence requirements to the self-energy with respect to the number of $\mathbf{k}$ points, bands, and plane waves. For that reason, we also apply an approximate treatment to compute the QP energies. This is the recently developed LDA-1/2 method,[32] which is based on the idea of Slater's transition state.[33,34] We apply this method by preparing a pd-like excitation in an electronic system for which XC is treated by the AM05 functional.[17] It leads to band structures for the group-III nitrides that around the fundamental gap and for the d bands of GaN and InN are in good agreement with measured spectroscopic data.[32,35] The computed fundamental energy gaps E_g in Table I are indeed close to the measured values. Other parts of the band structure, e.g. the energy positions of

TABLE I. Energy gap E_g and branch-point energies E_{BP} (with respect to the valence-band maximum) for zb and wz nitrides. For zb AlN, besides the direct Γ-Γ gap also the smaller indirect Γ-X gap is listed. The resulting absolute positions of the conduction band minimum E_c and valence band maximum E_v as well as the natural band discontinuities ΔE_c and ΔE_v between zb and wz are also given. The energy values have been derived from the QP eigenvalues computed within the HSE06+GW approach.[29] The corresponding values obtained from the LDA-1/2 treatment are given in parenthesis. Two different alignment methods have been applied to derive the band discontinuities. Besides the alignment via the branch-point energies, an additional alignment has been made in the LDA-1/2 framework using the spatially averaged electrostatic potentials whose differences $\Delta\bar{V} = 0.15$ (AlN), 0.01 (GaN), and 0.03 eV (InN) however remain small. The resulting band discontinuities are given as a second value in parenthesis. All values are in electron volt.

Compound	Crystal	E_g	E_{BP}	E_c	E_v	ΔE_c	ΔE_v
AlN	zb (Γ-Γ)	6.271 (6.176)	3.422 (3.489)	2.849 (2.687)	−3.422 (−3.489)	0.108 (0.098, 0.212)	−0.069 (0.058, −0.090)
	zb (Γ-X)	5.198 (5.429)		1.776 (1.940)		1.181 (1.045, 0.960)	
	wz	6.310 (6.331)	3.353 (3.546)	2.957 (2.785)	−3.353 (−3.546)		
GaN	zb	3.427 (3.514)	2.366 (2.556)	1.061 (0.958)	−2.366 (−2.556)	0.170 (0.154, 0.190)	0.062 (0.035, 0.022)
	wz	3.659 (3.703)	2.428 (2.591)	1.231 (1.112)	−2.428 (−2.591)		
InN	zb	0.414 (0.543)	1.487 (1.430)	−1.073 (−0.887)	−1.487 (−1.430)	0.131 (0.099, 0.104)	0.093 (0.069, 0.057)
	wz	0.638 (0.711)	1.579 (1.499)	−0.941 (−0.788)	−1.579 (−1.499)		

the lowest s-like valence bands and the total widths of the valence bands, come out less accurate with an underestimate of their binding energies. However, for the discussion of the lowest empty and highest occupied QP electronic states in the heterocrystalline structures, cubic inclusions in hexagonal matrices (modeled by the superlattices described above), the LDA-1/2 approximation[32] should give excellent results for the near-band-edge states. Since wz and zb nitrides are treated within exactly the same approximations, inaccuracies in interband distances, occurring eventually, should cancel each other to a large extent.

III. NATURAL BAND DISCONTINUITIES

In a first step, we calculate the band discontinuities ΔE_v and ΔE_c between the valence bands and conduction bands, respectively, of zb and wz nitrides. The positive sign of ΔE_v (or ΔE_c) indicates that the embedded cubic inclusion represents a quantum well for holes (or electrons) in the cubic regions. Thereby, $\Delta E_v \Delta E_c > 0$ describes a type-I hetero(crystalline)structure while $\Delta E_v \Delta E_c < 0$ gives rise to a type-II hetero(crystalline) structure. In a first step, we use a "macroscopic" approach,[36] which only requires the calculation of the QP band structures of the corresponding bulk compounds. The energy alignment of the two band structures for the cubic and hexagonal nitride polytypes asks for a common universal reference level. Frensley and Kroemer[37] suggested to use an internal reference level, which may be pinned at the interface in the presence of virtual gap states. It may be identified with the branch-point energy.[38,39] In the spirit of the Shockley-Anderson model,[40] the vacuum level takes over the role of the reference level if no interface states are present. The vacuum level is however strongly influenced by the electrostatic potential.

In a first step, we apply the branch-point energy E_{BP} of each material as common energy zero. At the branch-point energy, the band states change their character from predominantly acceptor-like (usually valence-band states) to mostly donor-like (usually conduction-band states) electronic states. According to Tersoff,[38] the related charge transfer leads to an intrinsic interface dipole that tends to lineup the energy bands at both sides of an interface in a way that the dipole itself vanishes. We compute the reference levels E_{BP} according to an approximate method that was successful for several material combinations.[36,39] The calculations have been performed using the QP band structure resulting from the full HSE06+GW scheme [see Fig. 3(a)] as well as the approximate LDA-1/2 method [see Fig. 3(b)]. For comparison, another band alignment based on the average electrostatic potentials $\bar{V}$ resulting from the LDA-1/2 approach for the zb and wz polytypes has been made. Although ionization energies and electron affinities are not explicitly derived, instead only the positions of the band edges E_c and E_v with respect to $\bar{V}$ are determined. This procedure yields the same results as the Shockley-Anderson model with the vacuum-level alignment.[40] We find that the displacements $\Delta\bar{V}$ due to the potential differences between zb and wz are small, $\Delta\bar{V} = 0.15$ eV (AlN), 0.01 eV (GaN), and 0.03 eV (InN). The second type of "natural" band discontinuities, ΔE_c and ΔE_v, arises from the absolute band-edge positions with respect to $\bar{V}$ in both polytypes.

The results for the band discontinuities ΔE_c and ΔE_v are given in Table I and Fig. 3 together with those for the fundamental energy gap E_g and the corresponding relative positions E_c and E_v of the conduction-band minimum (CBM) and the valence-band maximum (VBM), respectively. In the case of zb AlN, the indirect Γ-X gap and the conduction band position E_c at the X point are listed in addition to the direct Γ-Γ gap. The computed values are slightly different from those given in Ref. 36 mostly due to the different atomic geometries used. The geometries optimized here by means of the AM05 XC functional are closer to the experimentally determined structures. We find that the band discontinuities ΔE_v and ΔE_c between zb and wz are relatively small. Only the CBM at X in zb AlN exhibits a large distance of about 1 eV to the CBM at Γ of wz AlN. Thereby the absolute values of the band discontinuities are in general much larger in the conduction-band

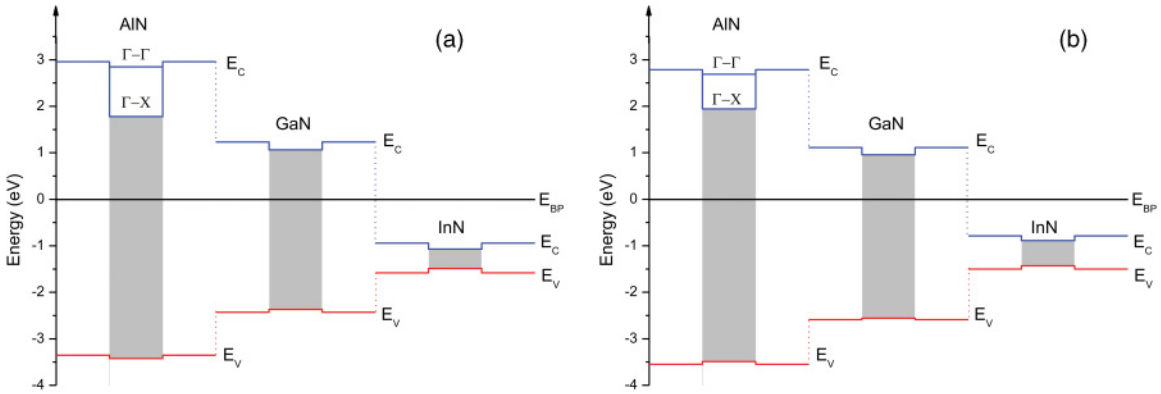

FIG. 3. (Color online) Band lineups for cubic inclusion embedded in hexagonal environment from QP calculations. The branch-point energy (here: energy zero) and the values from Table I have been used for alignment. Two different approximations, (a) full HSE06+GW and (b) approximate LDA-1/2, have been applied. The shaded areas illustrate the fundamental gaps in the regions of the cubic inclusions.

case whereas the valence bands are almost aligned (see also Table I). The combination of the two band-structure methods with the two alignment procedures described above yields three different sets of natural band discontinuities ΔE_c and ΔE_v given in Table I. The important information is that the values are only weakly dependent on the procedure. The average deviation of ΔE_c (ΔE_v) amounts to 36 meV (40 meV) for GaN and 32 meV (26 meV) for InN. Only for AlN the variation approaches larger values up to 0.1 eV for Γ-Γ or 0.2 eV for Γ-X. The positive signs indicate type-I heterocrystalline structures apart from the AlN case where the holes should not be localized within the cubic inclusion in two of the three approaches used. In the case of the AlN, cubic inclusions represent heterocrystalline structures of type II (at least within two procedures) where only the electrons are localized in the zb layers. The strength of the localization depends on the Γ or X character of the electrons. The almost vanishing valence-band offsets between cubic and hexagonal group-III nitrides do not indicate the validity of the common anion rule.[41] On the contrary, Fig. 3 clearly shows large valence-band offsets between two different wz group-III nitrides of about 0.93 (0.96) eV (AlN-GaN) and 0.84 (1.09) eV (GaN-InN) using the HSE06+GW (LDA-1/2) approach and the BP alignment of the order of measured values[42,43] despite the common anion.

The computed energy values in Table I are in rough agreement with other band-structure calculations, especially for AlN and GaN. Examples are the values $\Delta E_c = 0.162$ eV (AlN) and 0.154 eV (GaN) at Γ obtained from DFT-LDA computations without QP corrections.[44] Similar values of $\Delta E_c = 0.150$ eV (GaN) and 0.120 eV (InN) have been obtained by Yeh *et al.*[45] The absolute values for the valence-band offsets are much smaller and may vary in sign. For instance, Murayama and Nakayama[44] (assuming that no dipole potential exists across the interface) found $\Delta E_v = -56$ (AlN) and -34 (GaN) meV. Dalpian and Wei derived a value of $\Delta E_v = -22$ meV for GaN[46] by using the (KS) eigenvalues of the core levels as calculated within DFT-GGA. These valence-band discontinuities indicate a type-II heterocrystalline behavior which is different from the findings based on the alignment via the branch-point energy (cf. Table I). However, this difference can most likely be attributed to the QP corrections that are missing in Ref. 46. Using the KS eigenvalues of the Ga3d states (calculated within GGA) to perform the energy alignment, we also found $\Delta E_v < 0$ in agreement with Dalpian and Wei.

Using the averaged electrostatic potentials to achieve the energy alignment of the wz and zb band structures, contradictory results have been derived for the discontinuities within DFT-LDA. Stampfl and Van de Walle[7] predicted a type-II character with $\Delta E_c = 0.27$ eV and $\Delta E_v = -0.07$ eV for GaN. The DFT-LDA superlattice calculations of Majewski and Vogl[8] qualitatively agree with our findings for AlN and GaN (see Table I and Fig. 3). They also report a band lineup for zb/wz leading to a type-I junction.[14] The values obtained by Majewski and Vogl including (neglecting) atomic relaxations of the interfaces are $\Delta E_v = 0.02$ (-0.10) eV and $\Delta E_c = 1.30$ (1.40) eV for AlN and $\Delta E_v = 0.04$ (0.02) eV and $\Delta E_c = 0.12$ (0.14) eV for GaN. The small differences between the values outside and inside the parenthesis indicate a weak sensitivity to the details of the computations. Nevertheless, for unrelaxed interfaces with ($\Delta E_v = -0.10$ eV)[8] they also found a type-II heterocrystalline character for AlN, in contrast to the relaxed case. In a supercell calculation with slightly strained zb GaN, Majewski and Städele[47] confirmed the previous results with $\Delta E_c = 175$ meV and $\Delta E_v = 35$ meV for a type-I system. The results for GaN by Bandić *et al.*[48] are shifted with respect to those of Majewski and Vogl[8] since the interface dipole contribution described by the difference in electrostatic potentials is not taken into account.

Taking the accuracy of the band-structure and alignment methods into account, one has to point out that no final conclusion can be made for the valence-band lineup between cubic and hexagonal AlN. We have to point out that our results for GaN and InN, do not follow the simplified argument that the VBM of a pure compound in wz structure is usually higher than that in the zb structure.[46] This should be due to the crystal-field splitting, which moves the uppermost occupied wz level toward higher energies. Indeed, this effect is present. However, we claim that the discussion of the band structures of isolated polytypes is insufficient. Rather, one needs an alignment via a reference level that accounts for the electrostatics at the interface.

In summary, the manifold first-principles results ask for some comments: (i) in general, the (natural) valence-band

offsets ΔE_v between zb and wz for the three nitrides are small, $|\Delta E_v| \leqslant 0.1$ eV, independent of the approach that has been used for this estimation. Most important is the treatment of exchange and correlation in the underlying electronic-structure calculations. Conventional DFT results using GGA or local-density-approximation (LDA) functionals are less reliable on predicting valence-band offsets than hybrid functionals or, much better, hybrid-functional-based QP calculations.[49–51] (ii) The positive or negative values ΔE_v may depend on the internal or external reference level used to align the bulk bands on both sides of the zb/wz interface.

At first glance, the values $\Delta E_v > 0$ in Table I seem to violate the rule that the VBM in wurtzite should usually be higher in energy than that in zb crystals due to the crystal-field splitting and intervalence band repulsion that exist in wz.[46] However, the same alignment procedure and electronic-structure calculations lead to values $\Delta E_v < 0$ for conventional III-V compounds GaAs, InP, InAs, and InSb.[52] We conclude that the crystal field itself with lattice parameters $c/a > 1.633$ and $u < 0.375$ for conventional III-V compounds (crystallizing in zb under ambient conditions) in wurtzite geometry and $c/a \leqslant 1.663$ and $u > 0.375$ for III-nitrides (usually crystallizing in wz) obviously determines the sign of the small $|\Delta E_v|$ values.

IV. ELECTRONIC STRUCTURE OF HETEROCRYSTALLINE SUPERLATTICES

In the following, the predictions of band edges in zb-wz heterocrystalline systems by means of a branch-point alignment or the average electrostatic potential method (cf. Sec. III) are checked using electronic-structure calculations for real geometries. As described in Sec. II, the model system of a cubic inclusion $(ABC)_2$ in a hexagonal environment of layers $(AB)_6$ is studied in the form of a superlattice with a unit cell $(ABC)_2(AB)_6$ consisting of 18 cation-anion bilayers. The atomic geometries near the interfaces have been relaxed until the remaining forces are smaller than 1 meV/Å. The resulting quasiparticle-like LDA-1/2 band structures of the supercell systems are presented in Fig. 4 along two high-symmetry directions Γ-M and Γ-K of the two-dimensional (2D) Brillouin zone of a 2D hexagonal Bravais lattice. They correspond to the same directions in the wz crystals. In the cubic case, these directions perpendicular to the [111] direction correspond to $[2\bar{1}\bar{1}]$ and $[10\bar{1}]$. The $(2H)_6(3C)_2$ superlattice bands are compared to the QP bands of the wz nitrides projected onto the 2D BZ (shaded regions in Fig. 4). In the practical calculations, these shaded regions have been obtained by computing the superlattice bands of a $(2H)_9$ superlattice. The energy alignment of the band structures of the two superlattices $(2H)_6(3C)_2$ and $(2H)_9$ is made by aligning the laterally and vertically averaged electrostatic potentials of the two different superlattice systems. Details of the valence-band structures are shown in Fig. 5.

For all three nitrides, the superlattice band structures in Figs. 4 and 5 clearly indicate the appearance of localized states close to the band edges of the embedding hexagonal material as can be seen from the subbands in the fundamental gap of the projected wz band structure. For the bottom of the conduction bands near Γ, such subbands occur in a distance of about 0.40 (AlN), 0.15 (GaN), and 0.25 eV (InN). While for InN and GaN, only one electron subband occurs, three subbands are visible for AlN. This may be a consequence of the deeper quantum wells for bulk X-derived electronic states. As can be seen in Fig. 5, two twofold-degenerate (one two twofold-degenerate) hole subbands occur at Γ for InN (GaN). The uppermost nondegenerate band of the AlN superlattice is resonant with the $2H$ bulk bands. Only in certain distance from the Γ point it becomes of subband character. The reason for the different degeneracies of the uppermost bands is similar to that which causes a negative crystal-field splitting in AlN going from bulk zb to bulk wz with an ordering of the Γ_5 and Γ_1 valence states reversed to the GaN and InN cases. The maximum energy differences of the uppermost superlattice band at Γ to the pure $2H$ states amount to -60 (AlN), 65 (GaN), and 84 meV (InN).

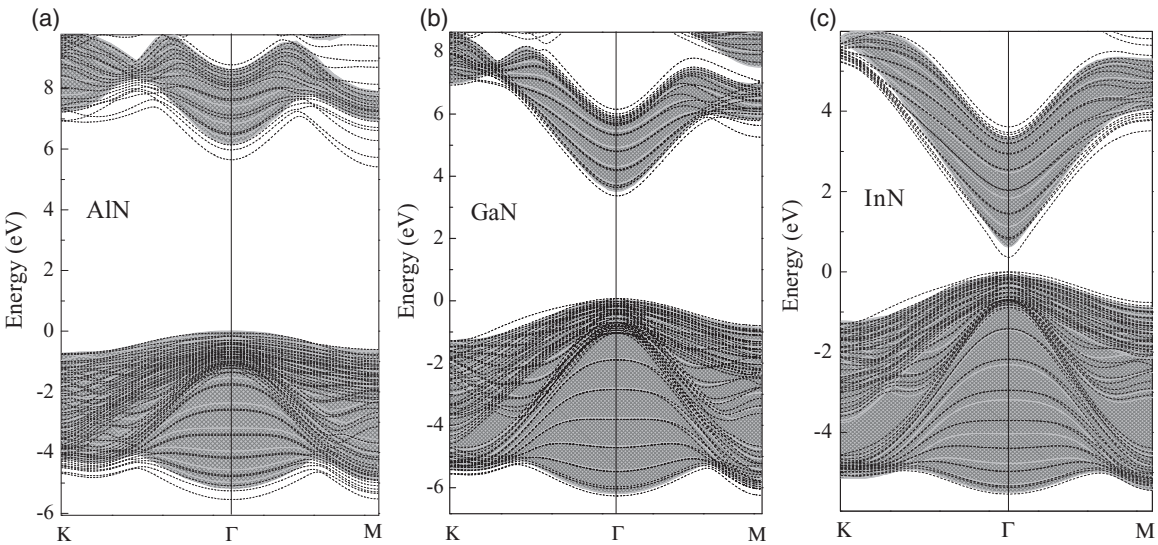

FIG. 4. (Color online) Band structure of $(2H)_6(3C)_2$ superlattice vs the 2D hexagonal BZ. The shaded region represents the projected bulk band structure of wurtzite crystal: (a) AlN, (b) GaN, and (c) InN.

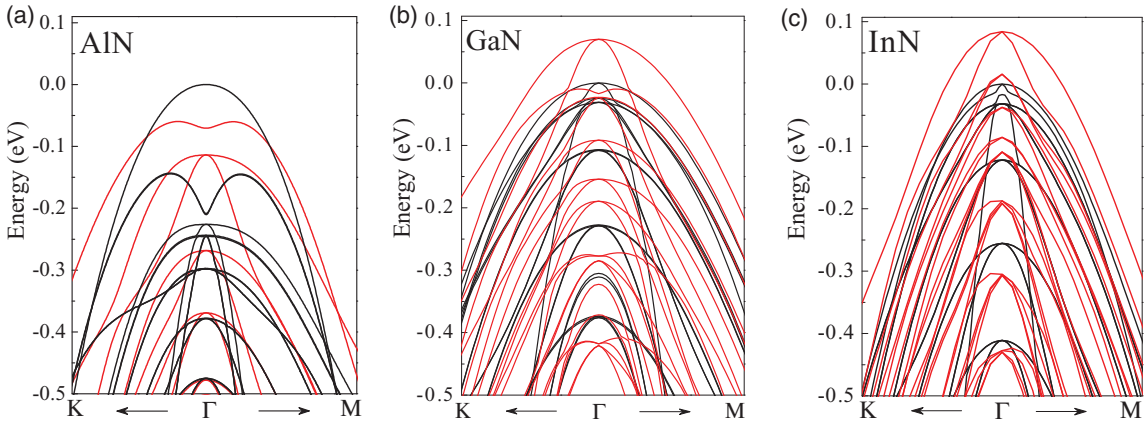

FIG. 5. (Color online) Top of the valence bands near Γ along the Γ-K and Γ-M directions. The black [red] lines represent bands of the $(2H)_6(3C)_2$ [$(2H)_9$] superlattices. The valence-band maximum of $2H$ is used as energy zero. (a) AlN, (b) GaN, and (c) InN.

At first glance, the subband structures seem to indicate type-I heterocrystalline structures for the cubic inclusions embedded in the hexagonal environment for GaN and InN while for AlN the band structure in Fig. 5(a) suggests type II. The characteristic subband energies with respect to the $2H$ band extrema also approach the order of magnitude of the values for the band discontinuities. Nevertheless, the simplified picture of rectangular quantum wells suggested by the band lineups in Sec. III has to be proven. There are two other pecularities in the AlN case. (i) The most probable type-II character suggested by the macroscopic approach is at least questionable outside the Γ region. (ii) The lowest electron subbands in Fig. 4(a) indicate an indirect character of the heterocrystalline structure. The absolute subband minima are situated at the M points of the hexagonal BZ. The indirect Γ-X gap of 5.482 eV is about 0.1 eV smaller than the direct Γ-Γ gap of 5.581 eV, reflecting probably the indirect character of bulk AlN. A third pecularity appears for GaN and InN. (iii) According to the simple picture of rectangular quantum wells for electrons and holes within the cubic regions the fundamental gaps of the superlattices $E_g(sl)$ are expected to be larger than the bulk gap $E_g(zb)$ of the cubic inclusions. The opposite is the case with $E_g(sl) = 3.30$ (0.35) eV and $E_g(zb) = 3.35$ (0.54) eV for GaN (InN). Such an inverted energetical ordering also seems to appear in measured spectra. Indeed, for GaN, a stacking fault luminescence at 3.27 eV, much below the zb gap, has been observed.[14]

Such observations ask for a clear interpretation. We focus on a discussion of the Figs. 4(c) and 5(c) for InN. Close to the Γ point there is only one electron subband, probably indicating that the quantum well in Fig. 3 is not deep enough and the thickness of the cubic inclusion is small. A rough estimate with an electron mass $m^* = 0.1m$ and a thickness of $d = 14.4$ Å yields a confinement energy in an infinite potential well of $\frac{\hbar^2}{2m^*}(\frac{\pi}{d})^2 = 1.24$ eV much larger than the band discontinuity $\Delta E_c = 0.13$ eV (Table I). This may qualitatively explain why in a real structure only one bound state exists. However, its energy of 0.24 eV below the conduction band minimum of $2H$-InN is larger than expected from the conduction band discontinuity. The reasons are real-structure effects and the stronger confinement due to the additional confinement in the triangular potential well induced by the built-in internal electric field due to the hexagonal-cubic interfaces (see below). As discussed above, apart from the AlN case, Figs. 4 and 5 also show hole bands very close to the top of the mapped $2H$ valence bands. The energy distance at Γ amounts to 0.08 eV for InN, a value that is much smaller than that for the electrons, seemingly in agreement with the much smaller quantum-well depth ΔE_v in Table I and Fig. 3. The tops of the superlattice valence bands at Γ are twofold degenerate. The threefold degeneracy of the bulk $3C$ electronic structure is lifted in the crystal field due to the reduced symmetry C^1_{3v} of $(2H)_6(3C)_2$, which is even lower than the C^4_{6v} symmetry of the hexagonal polytype $2H$.[16]

The stronger confinement of electrons and holes demonstrated in Figs. 4 and 5 in comparison to the corresponding quantum-well structures in Fig. 3 derived from the natural band discontinuities in Table I is due to additional electric fields E in the $3C$ and $2H$ layers within a superlattice period. They give rise to an additional macroscopic saw-tooth potential, as clearly demonstrated in Fig. 6, for the laterally averaged single-particle potential $V(z)$ in the superlattice system. In [111]/[0001] direction, the maxima and minima of the atomic oscillations in $V(z)$ decrease (increase) in the $3C$ ($2H$) part. This is a consequence of the interface charges between the two polytypes or the change ΔP between the spontaneous polarization field in $2H$ and the piezoelectric polarization field in $3C$. Parallel to the superlattice axis it holds[3,53]

$$\Delta P = -\varepsilon_0 \Delta E = -\frac{\varepsilon_0}{e}\left[\frac{d}{dz}V(z)\bigg|_{2H} - \frac{d}{dz}V(z)\bigg|_{3C}\right]. \quad (1)$$

For InN, the variation of $V(z)$ within a superlattice cell amounts to 0.25 eV. This leads to a change in the electric fields of $\Delta E = 2.2$ MV/cm or the polarization of $\Delta P = -1.9 \times 10^{-3}$ C/m^2. With 0.30 eV, $\Delta E = 2.9$ MV/cm and $\Delta P = -2.6 \times 10^{-3}$ C/m^2, the values are slightly larger for GaN. The electrostatic effect is more pronounced for AlN. We find a variation of the atomic oscillations through the superlattice of about 1.38 eV, which is almost by a factor 5 larger than in the InN heterocrystalline structure. The values for the electric field $\Delta E = 13.7$ MV/cm and polarization

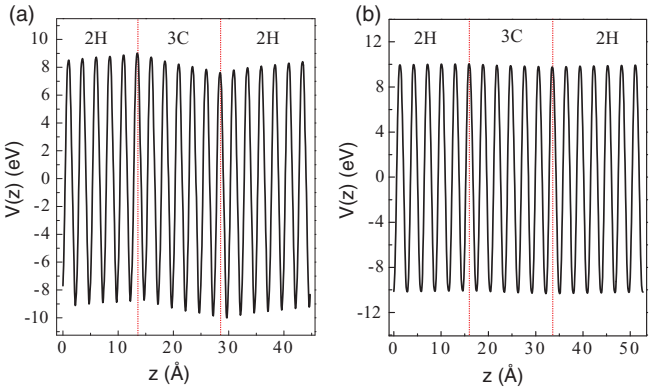

FIG. 6. (Color online) Laterally averaged single-particle potentials $V(z)$ along the superlattice axis. The atomic oscillations and the saw-tooth character of the envelope are clearly visible. The absolute minimum and maximum of the potential indicate the interfaces between cubic inclusion and hexagonal environment where the electrons or holes tend to be localized. (a) AlN and (b) InN. The potential for GaN is similar to that of InN.

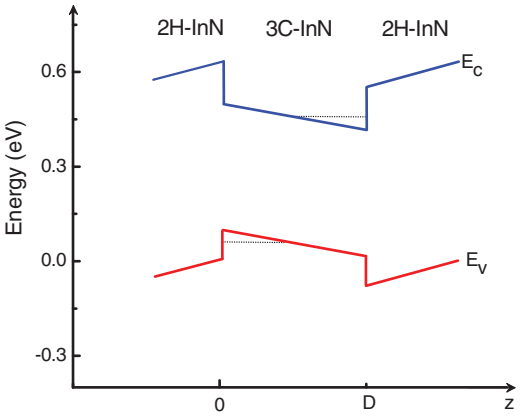

FIG. 7. (Color online) Band lineup for a thin $3C$ inclusion in an extended $2H$ matrix for InN (schematically). The internal electric field is taken into account. The lowest resulting electron and hole levels are indicated by horizontal dotted lines.

field $\Delta P = -12.1 \times 10^{-3}$ C/m^2 are correspondingly larger. This polarization value multiplied with the average electronic dielectric constant of the $3C$ and $2H$ polytypes[3] gives rise to spontaneous polarization fields (more precisely, the difference of spontaneous polarization in $2H$ and piezoelectric field in $3C$) of about -55×10^{-3} (AlN), -14×10^{-3} (GaN), and -16 (InN) $\times 10^{-3}$ C/m^2, smaller than the values of -81×10^{-3}, -29×10^{-3}, and -32×10^{-3} C/m^2 recommended by Vurgaftmann *et al.*[54] The underestimation of the polarization fields may be traced back to the presence of the piezoelectric field in the $3C$ regions.

The single-particle potentials in Fig. 6, especially the additional saw-tooth potentials, indicate that the picture of rectangular quantum-well structures with depths ΔE_c or ΔE_v shown in Fig. 3 is incomplete. The band lineups have to be modified by the additional saw-tooth potential. Consequently, the bottom of the quantum well for electrons and for the holes (at least for GaN and InN) has to be modified as schematically drawn in Fig. 7. The additional triangular potential wells have two effects on the electronic states: (i) the confinement of electrons and holes in the cubic inclusions is seemingly increased. (ii) In addition, the maxima of the wave-function squares are displaced against each other and hence reduce the optical-transition matrix elements. This effect is usually identified with the quantum confined Stark effect (QCSE).[55]

The latter effect is clearly demonstrated in Fig. 8 for the electrons. In Fig. 8, the wave-function squares of the lowest electron subbands and the highest hole subbands are plotted versus the heterocrystalline structure studied. States with relatively large in-plane kinetic energies with a wave vector representing an M point at the BZ boundary have been chosen. At least for electrons, the largest distances to the edge of the projected bulk bands and the largest number of subbands appear. The left panels in Fig. 8 for AlN, GaN, and InN clearly show the localization of the electron wave function in the area of the cubic inclusion. The tunneling of the wave functions through the $3C$-$2H$ interfaces into the wz regions is rather weak. The maximum of the probability to find an electron is displaced along the [111]/[0001] direction from its midwell position in a rectangular quantum well toward the upper interface. The results for the electrons are in complete agreement with the schematic band lineup drawn in Fig. 7.

However, for the holes, the simplified picture presented in Fig. 7 has to be strongly modified as shown in Fig. 8 (right panels). The maxima of the hole distributions appear near the lower $2H$-$3C$ interfaces, however at the $2H$ side, in contrast to the expectation from the rectangular quantum wells in Fig. 3 (perhaps with exception of AlN). The reason is the fact that the triangular quantum well due to saw-tooth potential in Fig. 7 is more important for holes, because the rectangular contribution defined by the barrier height related to ΔE_v is small.

For instance, for InN, the energy lowering of about 0.25 eV due to the QCSE is larger than the rectangular well (Fig. 3) with a natural band discontinuity $\Delta E_v = 0.09$ eV (Table I). As another consequence of the QCSE, the fundamental gap of the superlattice $E_g(sl) = 0.35$ eV is even smaller than the gap $E_g(zb) = 0.54$ eV of $3C$-InN. The findings for GaN and AlN also show the appearance of localized hole states in the $2H$ matrix. In the case of AlN with almost aligned top of the valence bands, the depth of the triangular polarization-field-induced quantum well is 1.38 eV, much more important than the rectangular contribution due to the small positive or negative value $\Delta E_v = 0.06/-0.09$ eV (Table I) of the natural band offset. The existence of an almost triangular potential well is also pointed out by the wave-function square, which indicates a high probability to find the hole on the $3C$ side and not only in the $2H$ region of the interface [see Fig. 8(a), right panel].

V. SUMMARY AND CONCLUSIONS

The electronic structure of cubic (zb) inclusions in hexagonal (wz) matrices has been studied by means of the QP electronic-structure theory and a superlattice method. The calculation of the natural band discontinuities ΔE_c and ΔE_v and the corresponding band lineup yields type-I hetero(crystalline) structures for InN and GaN, while a type-II character has almost been found for AlN. Thereby, the rectangular quantum wells of the electrons are relatively deep with $\Delta E_c = 0.1$–

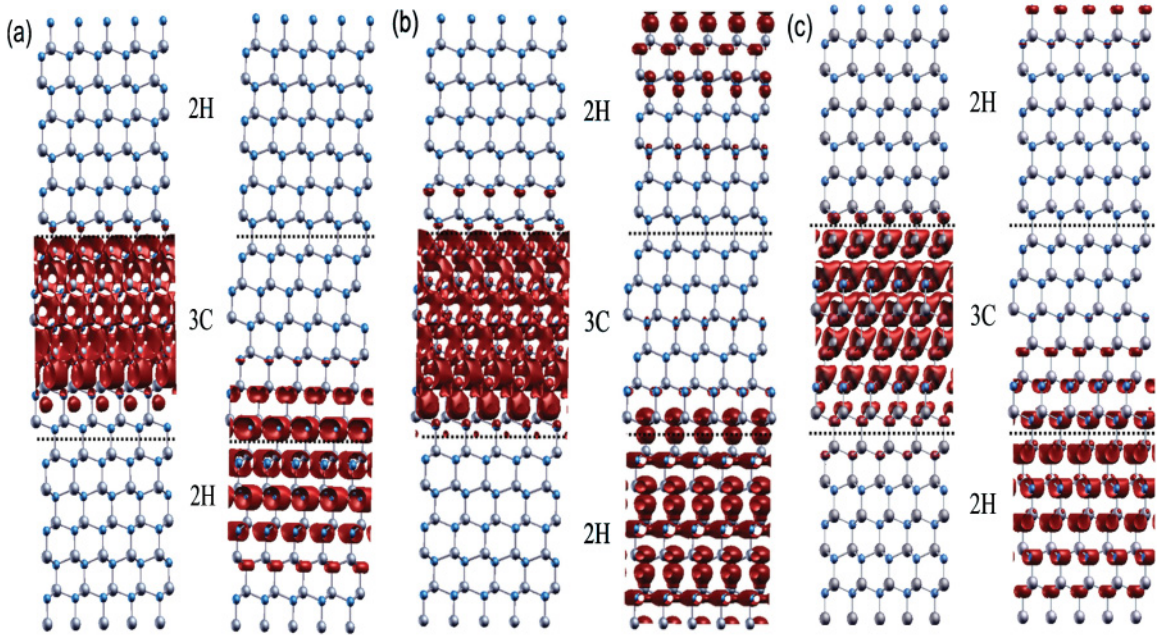

FIG. 8. (Color online) Wave-function squares of the lowest empty (left panel) and highest occupied (right panel) states at M together with two parallel $(11\bar{2}0)$ superlattices planes. The large circles represent cations whereas the small circles indicate nitrogen atoms. The nominal interfaces are indicated by dashed horizontal lines. (a) AlN, (b) GaN, and (c) InN.

0.3 eV. For X electrons in AlN with almost vanishing wave vectors, the value $\Delta E_c = 1.4$ eV is significantly increased. The situation for holes is completely different. The quantum wells in the cubic inclusions are rather flat for GaN and InN with $\Delta E_v = 0.06$ or 0.09 eV. For AlN, the value of ΔE_v is not exactly fixed and can even have a changed sign. However, the small $|\Delta E_v|$ do not indicate the validity of the common anion rule.

The predictions for the band lineups for cubic inclusions in hexagonal matrices have been proved by studying the electronic structure of such heterocrystalline structures within supercell geometries. For all group-III nitrides, AlN, GaN, and InN subbands of localized states within the fundamental gaps of the projected $2H$ band structures have been observed, a fact that seems to confirm the picture of the band lineups, at least for GaN and InN. However, a dramatic influence of the internal electric fields due to the pyroelectricity as well as piezoelectricity of the wz crystals and the piezoelectricity of the zb materials has been found. The localization of the electron states is displaced toward one of the two $3C$-$2H$ interfaces. The field effect on the hole states is more drastic. The maximum of the hole distributions has been observed near the other $3C$-$2H$ interface but not in the cubic inclusion, rather on the $2H$ side.

ACKNOWLEDGMENTS

We acknowledge financial support by the European Community within the EU ITN RAINBOW (Grant No. 2008-2133238) and the EU e-I3 ETSF (Grant No. 211956) as well as the Deutsche Forschungsgemeinschaft (Project No. Be 1346/20-1).

*abderrezak.belabbes@uni-jena.de
†bechsted@ifto.physik.uni-jena.de

[1] H. Amano, S. Kamiyama, and I. Akasaki, *Low Dimensional Nitride Semiconductors* (Oxford University Press, Oxford, 2002), Ch. 5, pp. 1–181.
[2] F. Bernardini, V. Fiorentini, and D. Vanderbilt, Phys. Rev. B **56**, R10024 (1997).
[3] F. Bechstedt, U. Grossner, and J. Furthmüller, Phys. Rev. B **62**, 8003 (2000).
[4] D. J. As, D. Schikora, and K. Lischka, Phys. Stat. Sol. (c) **0**, 1607 (2003).
[5] X. H. Wu, L. M. Brown, S. K. D. Kapolnek, B. Keller, S. P. DenBaars, and J. S. Speck, J. Appl. Phys. **80**, 3228 (1996).
[6] Z. Liliental-Weber, C. Kisielowski, S. Ruvimov, Y. Chen, J. Washburn, M. B. I. Grzegory, J. Jun, and S. Porowski, J. Electron. Mater. **25**, 1545 (1996).
[7] C. Stampfl and C. G. Van de Walle, Phys. Rev. B **57**, R15052 (1998).
[8] J. Majewski and P. Vogl, J. Nitride Semicond. Res. **3**, 21 (1998).
[9] F. Qian, Y. Li, S. Gradecak, D. Wang, C. J. Barrelet, and C. M. Lieber, Nano Lett. **4**, 1975 (2004).
[10] E. Calleja, J. Grandal, M. A. Sanchez-Garcia, M. Niebelschutz, V. Cimalla, and O. Ambacher, Appl. Phys. Lett. **90**, 262110 (2007).
[11] F. Werner, F. Limbach, M. Carsten, C. Denker, J. Malindretos, and A. Rizzi, Nano Lett. **9**, 1567 (2009).
[12] T. Akiyama, K. Sano, K. Nakamura, and T. Ito, Jpn. J. Appl. Phys. **45**, L275 (2006).

[13]P. Caroff, K. Dick, J. Johansson, M. Messing, K. Deppert, and L. Samuelson, Nat. Nanotechnol. **4**, 50 (2009).
[14]J. Renard, G. Tourbot, D. Sam-Giao, C. Bougerol, B. Daudin, and B. Gayral, Appl. Phys. Lett. **97**, 081910 (2010).
[15]V. Consonni, M. Knelangen, U. Jahn, A. Trampert, L. Geelhaar, and H. Riechert, Appl. Phys. Lett. **95**, 241910 (2009).
[16]F. Bechstedt and P. Käckell, Phys. Rev. Lett. **75**, 2180 (1995).
[17]A. E. Mattsson and T. R. Mattsson, J. Chem. Theory Comput. **5**, 887 (2009).
[18]L.C. de Carvalho, A. Schleife, F. Fuchs, and F. Bechstedt, Appl. Phys. Lett. **97**, 232101 (2010).
[19]G. Kresse and J. Furthmüller, Comp. Mater. Sci. **6**, 15 (1996).
[20]G. Kresse and D. Joubert, Phys. Rev. B **59**, 1758 (1999).
[21]H. J. Monkhorst and J. D. Pack, Phys. Rev. B **13**, 5188 (1976).
[22]L. Hedin, Phys. Rev. **139**, A796 (1965).
[23]L. Hedin and S. Lundqvist, in *Advances in Research and Applications, Solid State Physics*, edited by D. T. Frederick Seiz and H. Ehrenreich (Academic Press, 1970), Vol. 23, pp. 1–181.
[24]M. S. Hybertsen and S. G. Louie, Phys. Rev. B **34**, 5390 (1986).
[25]J. Heyd, G. E. Scuseria, and M. Ernzerhof, J. Chem. Phys. **124**, 219906 (2006).
[26]A. V. Krukau, O. A. Vydrov, A. F. Izmaylov, and G. E. Scuseria, J. Chem. Phys. **125**, 224106 (2006).
[27]J. Paier, M. Marsman, K. Hummer, G. Kresse, I. C. Gerber, and J. G. Ángyán, J. Chem. Phys. **124**, 154709 (2006).
[28]J. Paier, M. Marsman, K. Hummer, G. Kresse, I. C. Gerber, and J. G. Ángyán, J. Chem. Phys. **125**, 249901 (2006).
[29]F. Bechstedt, F. Fuchs, and G. Kresse, Physica Status Solidi (b) **246**, 1877 (2009).
[30]J. P. Perdew, K. Burke, and M. Ernzerhof, Phys. Rev. Lett. **77**, 3865 (1996).
[31]F. Fuchs, J. Furthmüller, F. Bechstedt, M. Shishkin, and G. Kresse, Phys. Rev. B **76**, 115109 (2007).
[32]L. G. Ferreira, M. Marques, and L. K. Teles, Phys. Rev. B **78**, 125116 (2008).
[33]J. C. Slater and K. H. Johnson, Phys. Rev. B **5**, 844 (1972).
[34]J. R. Leite and L. G. Ferreira, Phys. Rev. A **3**, 1224 (1971).
[35]A. Belabbes (unpublished).
[36]A. Schleife, F. Fuchs, C. Rödl, J. Furthmüller, and F. Bechstedt, Appl. Phys. Lett. **94**, 012104 (2009).
[37]W. R. Frensley and H. Kroemer, J. Vac. Sci. Technol. **13**, 810 (1976).
[38]J. Tersoff, Phys. Rev. B **30**, 4874 (1984).
[39]B. Höffling, A. Schleife, F. Fuchs, C. Rödl, and F. Bechstedt, Appl. Phys. Lett. **97**, 032116 (2010).
[40]F. Bechstedt and R. Enderlein, *Semiconductor Surfaces and Interfaces* (Akademie-Verlag, Berlin, 1988).
[41]J. O. McCaldin, T. C. McGill, and C. A. Mead, Phys. Rev. Lett. **36**, 56 (1976).
[42]C.-F. Shih, N.-C. Chen, P.-H. Chang, and K.-S. Liu, Jpn. J. Appl. Phys. **44**, 7892 (2005).
[43]P. D. C. King, T. D. Veal, P. H. Jefferson, C. F. M. Conville, T. Wang, P. J. Parbrook, H. Lu, and W. J. Schaff, Appl. Phys. Lett. **90**, 132105 (2007).
[44]M. Murayama and T. Nakayama, Phys. Rev. B **49**, 4710 (1994).
[45]C.-Y. Yeh, S.-H. Wei, and A. Zunger, Phys. Rev. B **50**, 2715 (1994).
[46]G. M. Dalpian and S.-H. Wei, Phys. Rev. Lett. **93**, 216401 (2004).
[47]J. A. Majewski and M. Städele, Mat. Res. Soc. Symp. Proc. **482**, 917 (1998).
[48]Z. Z. Bandić, T. C. McGill, and Z. Ikonić, Phys. Rev. B **56**, 3564 (1997).
[49]C. Mietze, M. Landmann, E. Rauls, H. Machhadani, S. Sakr, M. Tchernycheva, F. H. Julien, W. G. Schmidt, K. Lischka, and D. J. As, Phys. Rev. B **83**, 195301 (2011).
[50]P. G. Moses, M. Miao, Q. Yan, and C. G. V. de Walle, J. Chem. Phys. **134**, 084703 (2011).
[51]A. Alkauskas, P. Broqvist, F. Devynck, and A. Pasquarello, Phys. Rev. Lett. **101**, 106802 (2008).
[52]C. Panse, D. Kriegner, and F. Bechstedt, Phys. Rev. B **84**, 075217 (2011).
[53]A. Qteish, V. Heine, and R. J. Needs, Phys. Rev. B **45**, 6534 (1992).
[54]I. Vurgaftman and J. R. Meyer, J. Appl. Phys. **94**, 3675 (2003).
[55]Y.-H. Kuo, Y. K. Lee, Y. Ge, S. Ren, J. E. Roth, T. I. Kamnis, D. A. B. Miller, and J. S. Harris, Nature (London) **437**, 1334 (2005).